Knudsen effusion through polymer-coated three-layer porous graphene membranes

IOP Publishing Nanotechnology
Nanotechnology 28 (2017) 184003 (11pp) https://doi.org/10.1088/1361-6528/aa680f

Knudsen effusion through polymer-coated three-layer porous graphene membranes

Michael S H Boutilier, Nicolas G Hadjiconstantinou[1] and Rohit Karnik[1]

Department of Mechanical Engineering, Massachusetts Institute of Technology, 77 Massachusetts Avenue, Cambridge, MA 02139, United States of America

E-mail: ngh@mit.edu and karnik@mit.edu

Received 4 January 2017, revised 20 February 2017
Accepted for publication 20 March 2017
Published 10 April 2017

Abstract

Graphene membranes have the potential to exceed the permeance and selectivity limits of conventional gas separation membranes. Realizing this potential in practical systems relies on overcoming numerous scalability challenges, such as isolating or sealing permeable defects in macroscopic areas of graphene that can compromise performance and developing methods to create high densities of selective pores over large areas. This study focuses on a centimeter-scale membrane design, where leakage is reduced by substrate selection, permeable polymer film coating, and stacking of three independent layers of graphene, while (selective) pores are created by high density ion bombardment. The three-layer graphene provides high resistance to gas flow, which decreases with ion bombardment and results in selectivity consistent with Knudsen effusion. The results suggest that the permeable pores created in three layer graphene were larger than those required for molecular sieving and that designs based on single layer graphene may lend themselves more easily to molecular sieving of gases.

Keywords: 2D materials, ion irradiation, focused ion beam, poly(dimethyl siloxane) (PDMS), effusion, graphene membrane, gas separation

(Some figures may appear in colour only in the online journal)

1. Introduction

Graphene has been proposed as a potentially revolutionary membrane material [1–4] that could transform separation processes such as natural gas purification, hydrogen recovery, carbon capture, and desalination by offering enhanced permeance and selectivity [5–9]. Permeance decreases with membrane thickness, endowing molecularly thin materials such as graphene (thickness $\sim$0.34 nm) with a significant potential permeance advantage over the typical $\sim$100 nm active layer thickness in commercial polymer membranes [7]. Furthermore, graphene can support sub-nanometer pores, similar in size to small molecules or hydrated ions, enabling the possibility of molecule size based separation, yielding high selectivity.

This study focuses on graphene membranes for gas separation. Gas separation membranes are generally classified as dense or porous [7]. Conventional polymer membranes are dense membranes and operate by a solution-diffusion mechanism [10], in which bulk gas on the high pressure side is dissolved into the membrane, diffuses through the material, and emerges on the low pressure side (figure 1(a)) [6, 10–16]. Selectivity results from differences in gas solubility and diffusivity in the membrane.

Porous membranes, such as graphene [17] and graphene oxide (GO) membranes [18, 19], have defined passages throughout their volume [7]. When the pore diameter is on the same order or smaller than the kinetic diameter of the gas molecule, gas transport is in the molecular sieving regime (figure 1(a)) [11]. In this regime, pores are sufficiently small that the flow of larger gas molecules is strongly impeded compared to smaller gas molecules, resulting in high selectivity. For membranes with pores larger than a few kinetic diameters but still much smaller than the mean free path in the gas, and in the absence of strong molecule affinity effects, gas flow is in the Knudsen effusion regime (figure 1(a)) [11, 20]. In this regime, all gas molecules are able to traverse the membrane pores, with (modest) selectivity, which we will

[1] Authors to whom any correspondence should be addressed.

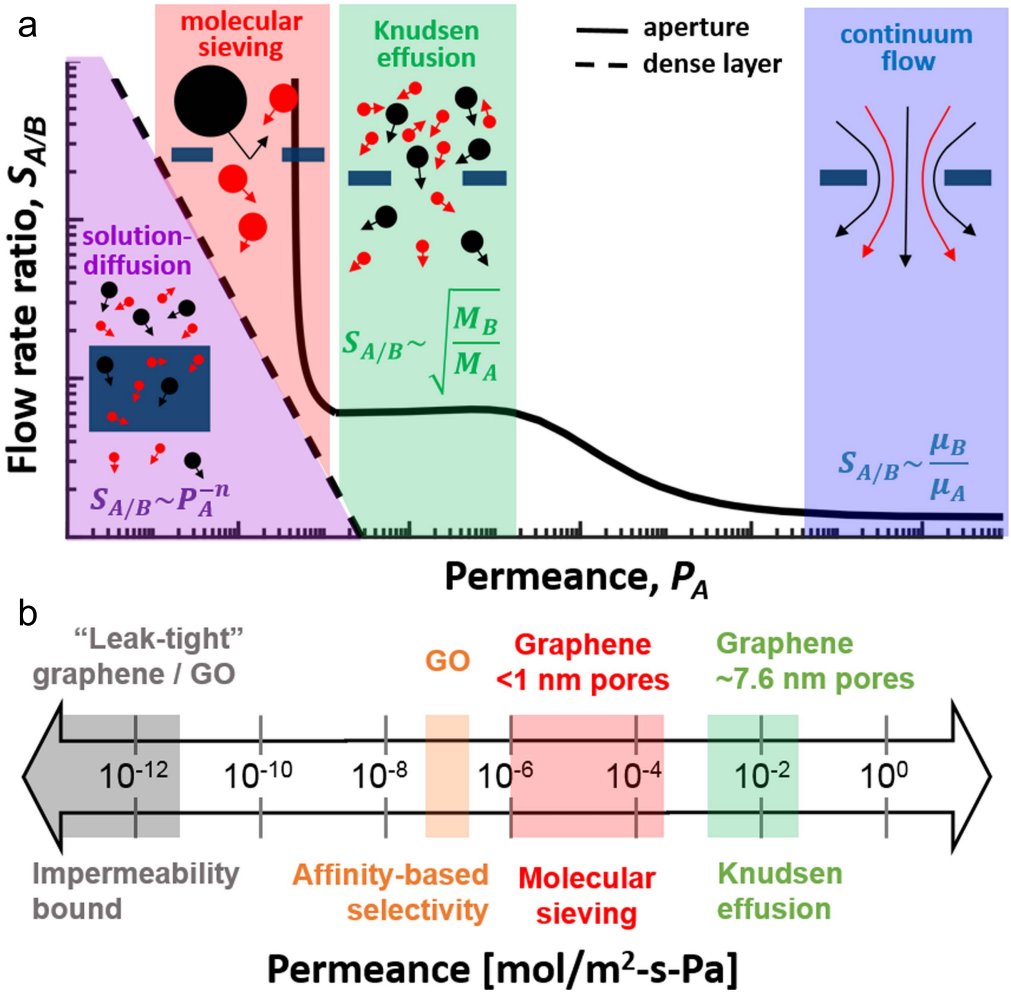

Figure 1. Membrane gas transport. (a) Sketch of gas permeance regimes for porous and dense membranes. The solid curve illustrates the variation in flow rate ratio with permeance through a pore in a thin membrane. Increasing the pore size increases permeance at the expense of selectivity. The dashed curve illustrates the Robeson [11] upper bound on polymer membrane performance. In this illustration, the flow rate ratio is for single species gas measurements, consistent with the measurements performed in this study. The sketch is for arbitrary gases A and B, where it is assumed that gas A is smaller and lighter than gas B, and has a higher permeance through the solution-diffusion membrane material. Here, μ_A is the viscosity of gas A, M_A is its molecular mass, and P_A is its permeance. $S_{A/B}$ is the ratio of the permeance of gas A to that of gas B, and n is a phenomenological constant in the Robeson upper bound that depends on the gas pair. (b) Approximate permeance ranges for graphene and GO membranes. Explicitly shown: the measured lower bound on permeance for pristine graphene by Bunch *et al* [31] and 'leak-tight' GO by Nair *et al* [19]; highly selective GO membranes, operating by an affinity-based separation mechanism, produced by Li *et al* [32]; near Knudsen effusion using an array of ~7.6 nm pores achieved by Celebi *et al* [20]; estimated permeance range for graphene and other two-dimensional materials with <1 nm pores, suitable for molecular sieving, based on reported experiments [9, 22, 23] and simulation data [2–4, 24].

refer to as Knudsen selectivity, resulting from the fact that molecules with smaller molecular mass move at higher average speeds than molecules with larger molecular mass. The Knudsen selectivity for arbitrary gas A over gas B is given by $S_{A/B} = \sqrt{M_B/M_A}$, where M_A and M_B are the molecular masses of the two gases. As the pore size is increased above the mean free path of the gas molecules, the transport mechanism transitions from the Knudsen regime to continuum flow (figure 1(a)) [21]. In this limit, transport rates are governed by viscosity.

Ideally, graphene membranes need to have large area with a high density of sub-nanometer pores that operate in the molecular sieving regime. This would provide high selectivity and high permeance at a practical scale. Molecular sieving based gas separation has been demonstrated through single or few pores in micron-scale areas of graphene by Koenig *et al* [22]. This was accomplished by first showing that pristine graphene is essentially impermeable to gases including helium [1] (the permeance was bounded from above by $\sim 10^{-12}$ mol m^{-2} s^{-1} Pa^{-1}, figure 1(b)) and then perforating the graphene by UV-ozone etching [22]. Following pore creation, hydrogen/methane selectivity of greater than 10^4 was measured. The available experimental data [9, 22, 23] and simulation results [2–4, 24] for graphene and other two-dimensional membranes suggest a potential permeance of $\sim 10^{-6}$–10^{-4} mol m^{-2} s^{-1} Pa^{-1} in the molecular-sieving regime (figure 1(b)). High gas permeance through graphene was later demonstrated by Celebi *et al* [25] using an array of ~7.6 nm pores with 4% porosity on a transmission electron microscopy (TEM) grid generated using a helium ion beam.

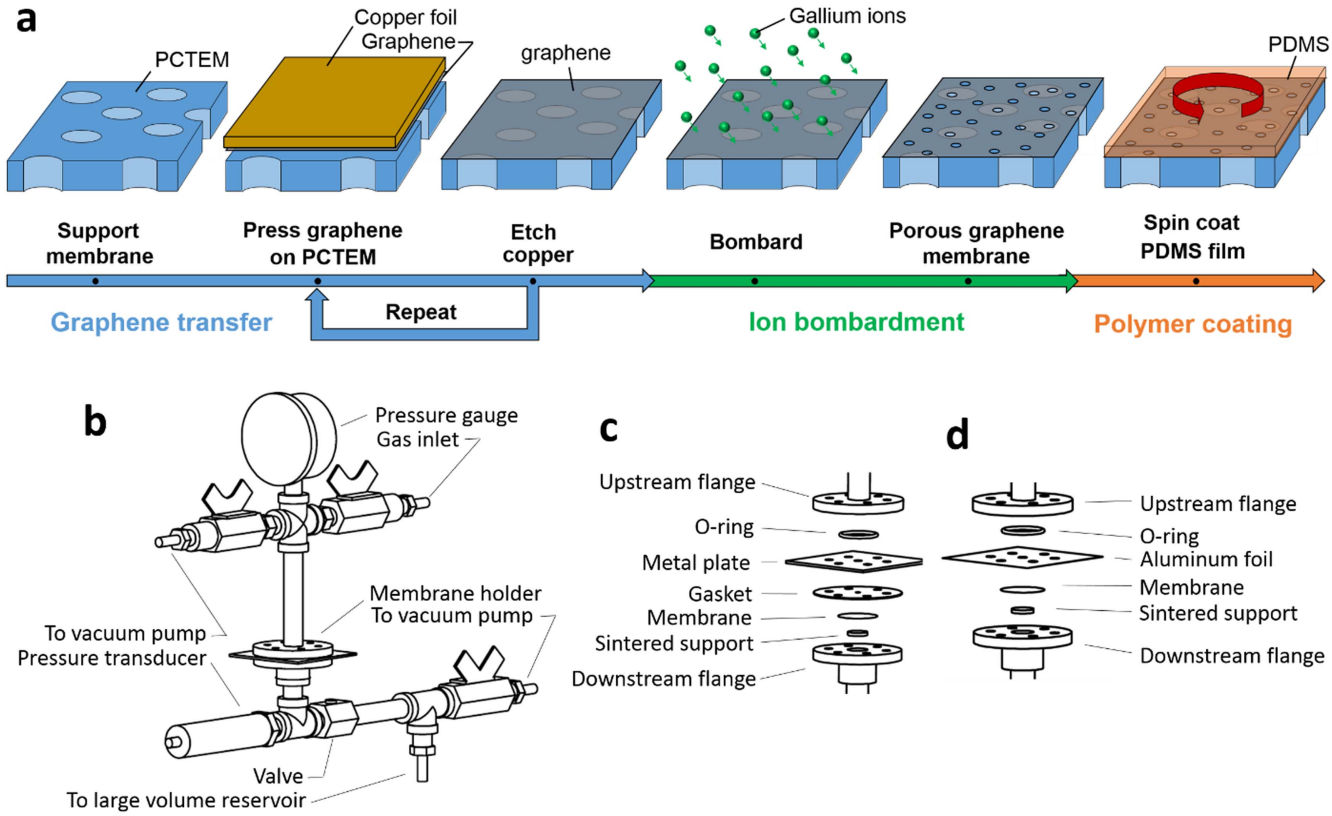

Figure 2. Membrane fabrication and gas permeance measurement. (a) One to three layers of graphene are transferred onto a PCTEM, bombarded with ions to increase graphene porosity, and then coated with a polymer layer. (b)–(d) Gas permeance measurement setup (b) and membrane holder assembly for membranes without (c) and with (d) a polymer coating. In the metal plate (c) and aluminum foil (d), the central holes, measuring 3 and 5 mm in diameter, respectively, define the exposed membrane area available to gas flow. The surrounding six bolt holes facilitate clamping of the membrane between the upstream and downstream flanges.

These pores are much larger than gas molecules, of size typically <0.6 nm [26], but still provide a modest hydrogen/carbon dioxide mass-based selectivity of ~3.4 (the Knudsen effusion limit for this pair is 4.7); the permeance of this Knudsen effusion-based membrane was $\sim 10^{-2}$ mol m^{-2} s^{-1} Pa^{-1} (figure 1(b)), four orders of magnitude higher than conventional polymer membranes with comparable selectivity.

Scaling these membranes up to practical sizes presents significant challenges. Most notable are the presence of defects in large areas of graphene, which produce non-selective leakage paths through the membranes [27–30], and the need for methods of producing dense arrays of selective nanopores over large areas. In this study we examine the performance of a particular graphene membrane design, fabricated and measured at the centimeter-scale, in which three layers of graphene and a polymer coating are used to minimize leakage, and pores are created by ion irradiation. The membrane is sufficiently large that the challenges of leakage and pore creation associated with realizing graphene membranes on industrial scale are also relevant here.

2. Experimental methods and materials

In the membrane design considered, graphene is transferred onto a support, perforated by high density ion bombardment, and then coated with a permeable polymer film to mitigate leakage flow.

2.1. Graphene transfer

Chemical vapor deposited (CVD) graphene (ACS materials) was transferred from copper onto polycarbonate track etched membrane (PCTEM) supports by the procedure described in [27] (figure 2(a)). PCTEMs have a smooth surface covered in an array of pores of a chosen diameter, in this case, 200 nm. Transferring graphene onto this support results in a parallel array of 200 nm diameter graphene membranes.

Graphene from the back side of the copper foil was first removed by floating the copper on copper etchant (ammonium persulfate; Transene, APS-100) for 5 min. The top side of the foil (with graphene) was then pressed against a 200 nm pore diameter PCTEM (Sterlitech, 200 nm, polyvinylpyrrolidone-free) by placing the PCTEM and graphene on the copper between glass slides and gently rolling a Pasteur pipette over the slide. This causes the graphene on copper to adhere to the PCTEM, which is then floated copper-side-down on ammonium persulfate until the copper is fully

removed, leaving a single layer of graphene on the PCTEM (figure 2(a)). The membrane is then rinsed in water, soaked in ethanol, and air dried.

This procedure is repeated to transfer additional layers of graphene, one at a time, on top of the graphene on PCTEM, stacking graphene layers on one side of the membrane. One to three layer graphene membranes were prepared in this way and measured in this study.

2.2. Ion bombardment

After transfer onto the PCTEM, pores were created in the graphene by bombardment with gallium ions in an FEI Helios Nanolab DualBeam 600. Bombardment was performed by acquiring 4096 × 3536 pixel images with the ion beam at a working distance of 4 mm, 100× magnification, 19 nA current, 8.0 kV voltage (unless otherwise specified), and at 52° to the ion beam (figure 2(a)).

2.3. Polymer film coating

Following ion bombardment, the graphene was coated with a thin polymer film (figure 2(a)). PDMS (polydimethylsiloxane, Sylgard 184) was mixed with a 10:1 elastomer/curing agent ratio and degassed in vacuum for 1 h. The membrane was secured to a glass slide with Kapton tape on all edges. The membrane was placed in a spin coater and accelerated to 8000 rpm. PDMS was pipetted onto the membrane (0.5 ml) and rotation continued for 10 min. The membranes were cured for 3 h at 76 °C. A razor blade was used to cut the membrane just inside the tape to remove it from the glass slide.

2.4. SEM imaging

SEM images of the membranes were obtained with an FEI Helios Nanolab DualBeam 600 at 2 kV, 86 pA, in immersion mode, employing an Everhart–Thornley detector. Carbon tape was used to make a conductive path from the graphene to the SEM stub. Cross sections of the PCTEM with graphene and PDMS were prepared by sectioning the membrane with a razor blade, then sputter coating with 2 nm of 80%/20% platinum–palladium.

2.5. Gas permeance measurements

Membrane permeance was measured using the apparatus shown in figures 2(b)–(d). The membrane was mounted in the holder positioned between an upstream gas line and downstream reservoir. Both sides of the membrane are initially pumped to below 0.01 psi. A single component gas is then supplied at constant pressure (1 atm) upstream. The pressure rise in the downstream reservoir is measured using a pressure transducer. The slope of the pressure time history was converted into a flow rate to determine permeance using the ideal gas law. Valves in the downstream reservoir can be used to restrict the volume from ∼100 l, to ∼4 l or ∼0.01 l, allowing accurate measurement of permeances over several orders of magnitude.

Two types of membrane holder were used. For membranes without PDMS, a metal plate pressed a Viton gasket against the membrane to create a seal (figure 2(c)). 3 mm holes in the centers of both the plate and gasket defined the flow area. Membranes with PDMS coatings have significantly lower permeance requiring a tighter seal. For these membranes, a piece of aluminum foil with a 5 mm hole in the center sealed the membrane and defined the flow area (figure 2(d)) [33]. Epoxy (ITW Devcon, 5 min Epoxy) between the membrane and tape as well as around the circumference of the hole in the tape created a seal. In both holders, the membrane is supported on the backside with a porous sintered steel support (∼2 μm pore size, Mott Corp.) and a 25 mm Viton O-ring sealed the upstream side of the flow cell against the aluminum tape or metal plate.

Gas flow rate measurements were performed on helium (He) and sulfur hexafluoride (SF_6). These gases have a wide difference in kinetic diameter (2.6 versus 5.5 Å) and molecular weight (4 versus 146 g mol^{-1}), which are key factors determining gas flow rates in the relevant transport regimes in this study.

Measurements were performed on separate sets of membranes after graphene transfer, after ion bombardment, and after polymer coating, since each of these steps accomplishes a specific design function.

3. Results

3.1. Intrinsic gas permeance of large area graphene

Transfer of graphene onto a PCTEM creates a composite membrane consisting of an array of 200 nm diameter graphene membranes (figures 3(a), (b)). The PCTEM provides mechanical support for the graphene and separates gas transport into parallel channels, helping to reduce leakage flow through tears in the graphene. These tears are visible in single layer graphene in figure 3(a). While graphene covers the majority of 200 nm PCTEM pores, some underlay large tears in the graphene that leave those PCTEM pores open to gas flow. In this image, a large tear extends across the diagonal from the lower left corner to the upper right corner. All of the PCTEM pores along this tear have large openings to gas flow.

These tears make the membrane gas permeable even before it is intentionally perforated (figure 3(c)). By separating gas flow through the graphene into a large number of parallel PCTEM pores, the membrane design is able to reduce this leakage. The complete structure can be modeled as a gas flow resistance network as shown in figure 3(d). Gas flow can either pass through tears in the membrane, where the only resistance to flow is due to the support PCTEM pores (R_{PCTEM}), or through areas nominally covered by graphene, where it experiences the resistance to flow through the graphene ($R_{Graphene}$) and then through the support PCTEM. Here, γ, the graphene coverage, is the fraction of support pores without tears in the overlying graphene. Adding resistance 'in series' with the tears and isolating them from areas with

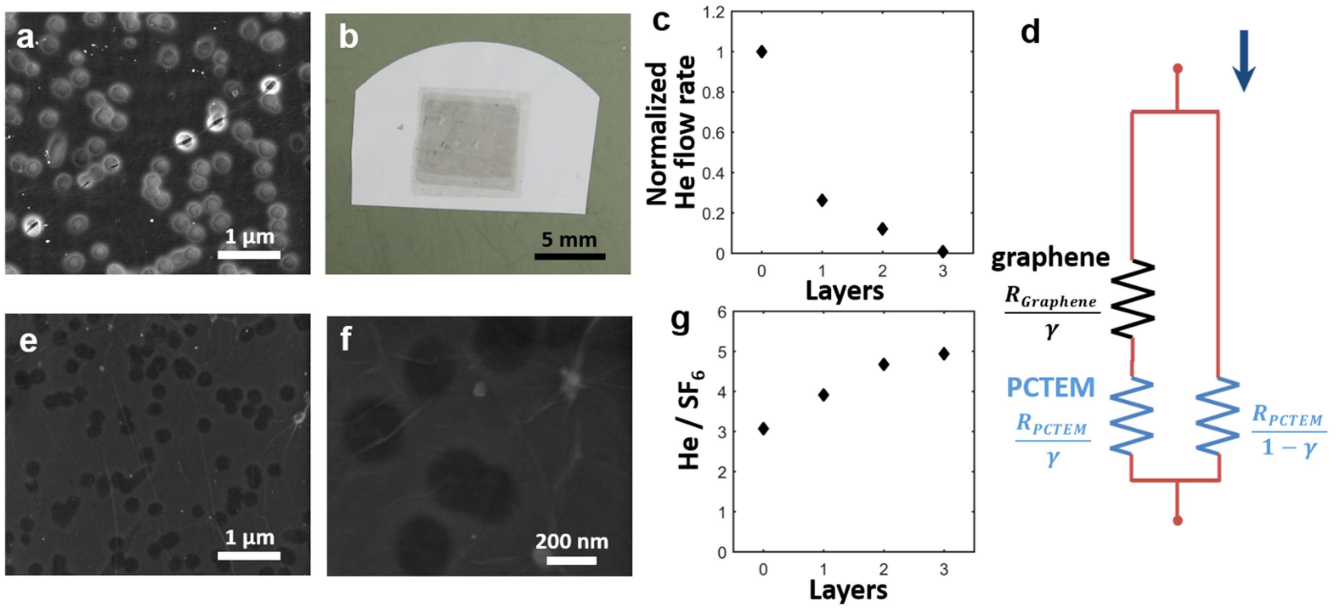

Figure 3. Graphene on PCTEM. (a) SEM image of a single layer graphene membrane. (b) Photograph of a three layer graphene membrane. (c) Helium permeance as the number of graphene layers increases. Permeance is normalized by the value for a PCTEM without graphene. (d) Simple equivalent flow rate resistance model for graphene membranes without a polymer coating. (e), (f) SEM images of three layer graphene membranes. (g) Measured He/SF_6 flow rate ratio as the number of graphene layers increases.

graphene has the effect of reducing leakage through tears. Without such a structure, tears in the graphene would further impair the graphene barrier performance.

Leakage is further reduced by stacking additional layers of graphene over the membrane (figure 3(c)), such that tears in one layer are likely to be covered by graphene in another layer. This effectively increases the graphene coverage, γ. SEM images illustrate that three layer membranes have fewer visible tears (figures 3(e), (f) compared to figure 3(a)). However, tears in different layers will align over some PCTEM pores, resulting in passages for gas transport [27]. As a result, centimeter-scale multi-layer graphene membranes also have an inherent permeance, albeit diminishing with increasing number of graphene layers (figure 3(c)) [27]. Transfer of three layers of graphene onto PCTEM reduces helium flow by more than 99% compared to a bare 200 nm pore PCTEM without graphene.

Reducing leakage from tears also has the effect of mildly increasing the ratios of flow rates of different gases through the membrane (figure 3(g)). Specifically, the He/SF_6 flow rate ratio increases from ~3.1 for a bare PCTEM to ~4.9 for a three layer PCTEM. The reason for this increase is that, in addition to the micron-scale tears visible in SEM images (figure 3(a)), CVD graphene features nanometer-scale gas permeable defects [27, 28]. Unlike micron-scale tears, which produce effectively zero graphene resistance over the PCTEM pore, these smaller defects have significant resistance. As the number of layers of graphene is increased, the fraction of leakage flow passing through micron-scale tears decreases while that through nanometer-scale defects increases. By virtue of their size (~6.5 nm size on average [27, 28]) relative to the gas mean free path (~140 nm for He and ~30 nm for SF_6 at standard conditions), nanometer-scale defects operate in the Knudsen effusion regime. On the other hand, tears are larger than the mean free path of the gas molecules, and thus have lower selectivity than defects. Consequently, as the number of layers of graphene increases, and a greater fraction of the flow passes through defects, selectivity increases. However, because defects in this graphene are much larger than the gas molecule size (0.26 nm for He and 0.55 nm for SF_6), the inherent selectivity of these membranes is limited to the Knudsen selectivity, i.e., $<\sqrt{M_{SF6}/M_{He}} \sim 6.0$. This is consistent with the saturating flow rate ratio trend observed in figure 3(g).

3.2. Pore creation by ion bombardment

Methods to create large, dense arrays of pores in graphene are needed to develop graphene membrane technology on useful scales. Here, we evaluate the use of high density ion bombardment for this purpose.

High energy ion bombardment can damage the graphene lattice creating single or multi-vacancy defects [34, 35]. Single and three layer graphene membranes were bombarded at densities ranging from 10^{13} to 10^{15} ions cm^{-2} (figure 4). At sufficiently high densities, gallium embedded in the PCTEM makes the bombarded areas visible (figure 4(a)). Flow rate increases significantly between 10^{14} and 10^{15} ion cm^{-2} bombardment (figures 4(b), (c)), without an increase in flow rate ratio (e.g., figure 4(d)), suggesting that large pores or damaged regions are being created in graphene at these bombardment densities. In fact, the flow rate ratio through three layer membranes decreases towards the value for a bare PCTEM, providing further evidence that the graphene is developing large openings at these bombardment densities (figure 4(d)).

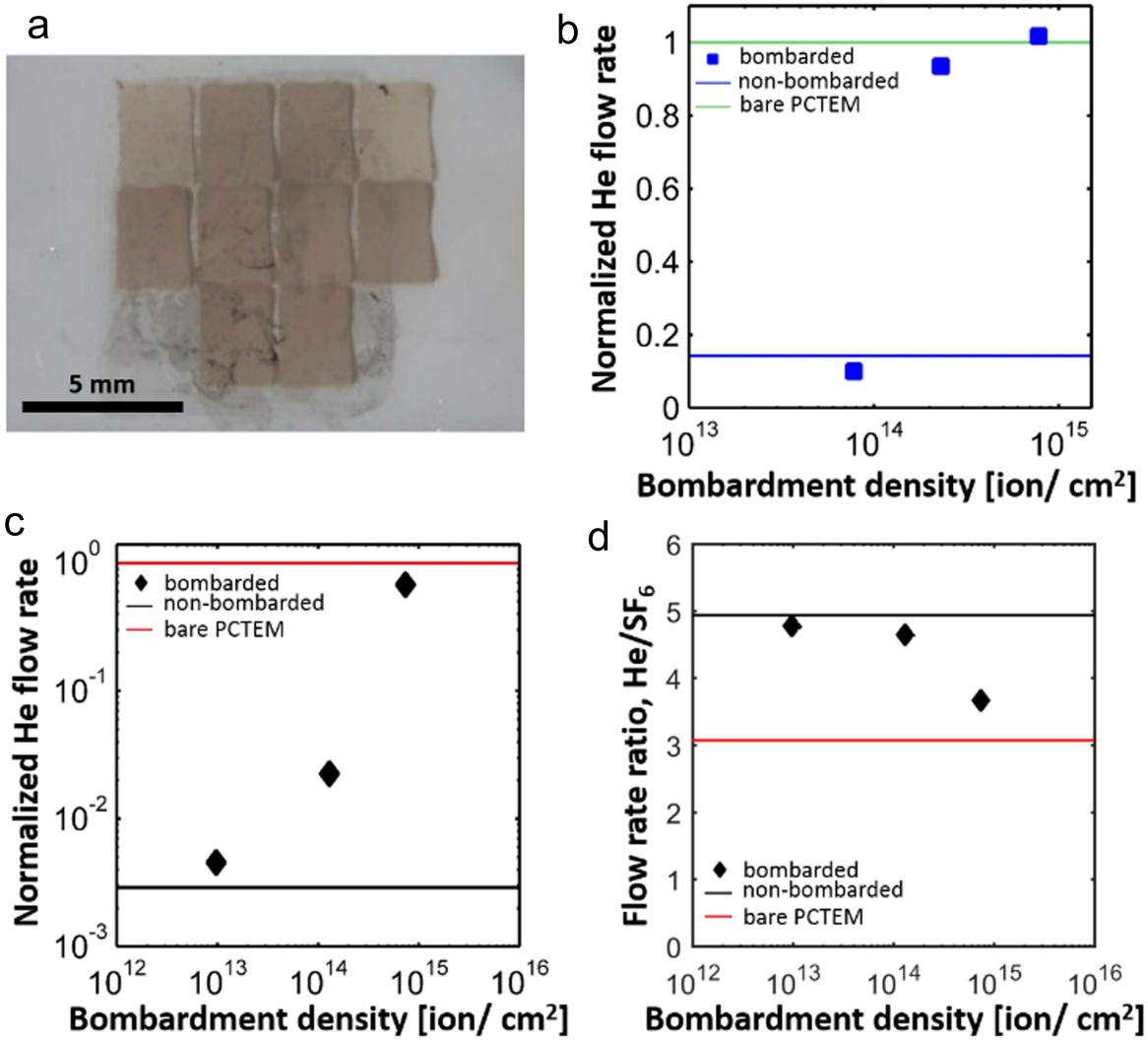

Figure 4. Ion-bombarded graphene. (a) Photograph of a graphene membrane bombarded at 4×10^{15} ion cm^{-2} (except in the top corners, where the density is 2×10^{15}). (b), (c) Gas flow rates through graphene bombarded at 52°. (b) One-layer graphene on 10 nm pore diameter PCTEM (bombarded at 8 kV). (c) Three-layer graphene on 200 nm pore diameter PCTEM (bombarded at 1 kV, 5 kV, and 16 kV for densities of $\sim 10^{13}$, $\sim 10^{14}$, and $\sim 10^{15}$ ion cm^{-2}, respectively). (d) Flow rate ratio corresponding to the three-layer graphene membranes.

The results in figure 4 can be further understood by considering the equivalent gas resistance model of figure 3(d). Ion bombardment creates pores in the graphene, reducing its resistance to gas flow (R_{Graphene}) and possibly changing its selectivity. However, if the pores created in graphene have low permeance or density, the resistance to gas flow through the graphene remains higher than through the PCTEM pores beneath tears ($R_{\text{Graphene}} \gg R_{\text{PCTEM}}$). As a result, gas flow is dominated by leakage and ion bombardment will not measurably change the membrane permeance or flow rate ratio. This could be occurring at low bombardment densities ($\sim 10^{13}$) in figure 4. At bombardment densities that are sufficiently large to reduce the graphene resistance to near the PCTEM resistance ($R_{\text{Graphene}} \sim R_{\text{PCTEM}}$), the pore size in graphene may be too large for molecular sieving or even Knudsen effusion, resulting in a lower gas flow rate ratio.

Alternative pore creation methods to create a higher density of small pores, reducing R_{Graphene} at high selectivity, could resolve this issue. Approaches such as bombardment with small ion clusters or intentionally introducing impurities to grow pores during graphene synthesis may offer better control over this process. Methods to seal micron-scale tears [36] and/or nanometer-scale defects in graphene could also remedy the problem. This would reduce leakage flow compared to that through the graphene pores, potentially allowing for significant graphene permeance at low bombardment densities where the created pores may be selective.

Instead of approaches akin to the ones described above, which effectively increase γ, here we consider effectively increasing the support pore resistance (R_{PCTEM}) in an effort to bring its value closer to the flow resistance of bombarded graphene (R_{Graphene}, figure 3(d)). As ion bombardment density increases, we expect the size and density of the pores it creates to increase, which will reduce not only the resistance of the porous graphene (R_{Graphene}), but also its selectivity. Therefore, selectivity is expected for high values of R_{Graphene}. A higher R_{PCTEM} would result in measureable selectivity of the overall membrane for higher values of

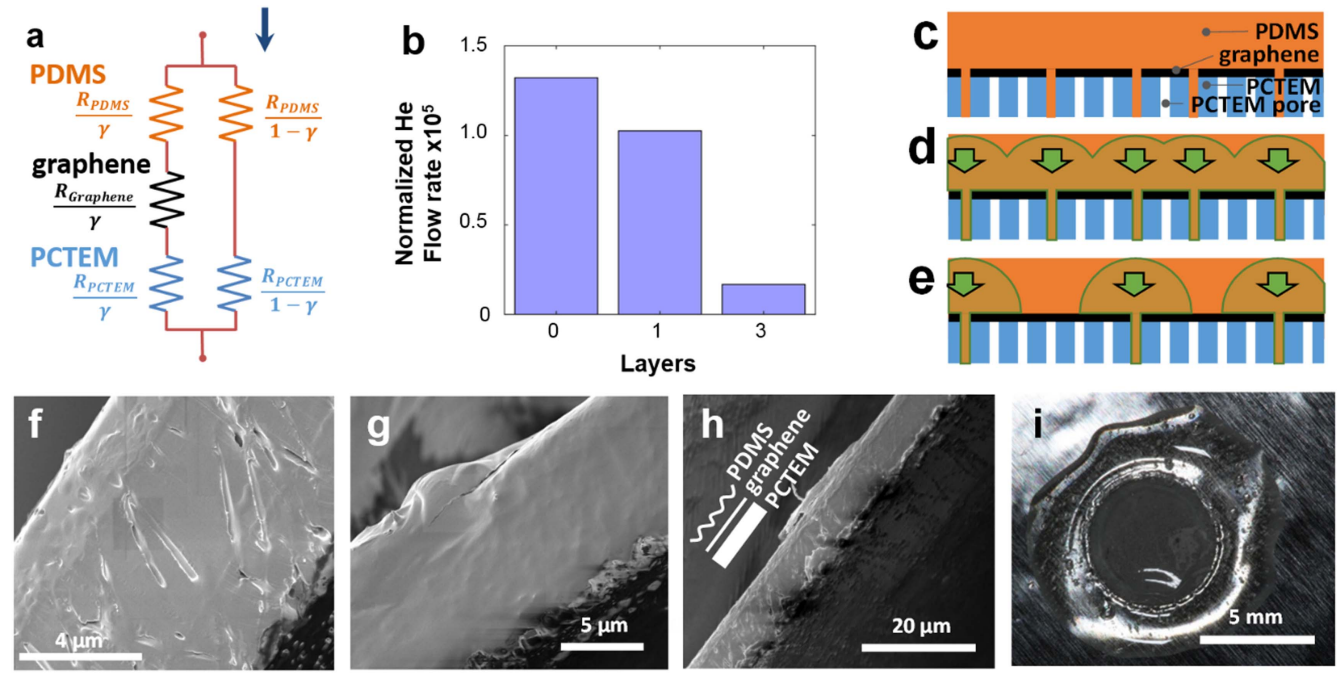

Figure 5. Polymer film-coated graphene membrane. (a) Simple equivalent flow rate resistance model for graphene membranes with a polymer coating. (b) Gas flow rates through PCTEM with and without graphene, after PDMS spin coating. Flow rates normalized to the value for a PCTEM without graphene or PDMS. (c) Sketch of PDMS filling of PCTEM pores beneath tears in the graphene. (d), (e) Sketches of gas flow spreading in the PDMS film. With higher tear density (e.g., in single layer graphene), gas flow spreading in the PDMS results in cross-talk between PCTEM pores (c), whereas, at lower tear density (e.g., in three layer graphene), the PCTEM pores remain isolated (d). (f)–(h) Cross-section images showing the stack, from left to right, of PDMS, graphene, and PCTEM, as illustrated in the inset of (h). These images are for a low quality graphene transfer, showing areas with graphene coverage (f) and without graphene coverage (g). Note that the three-layer graphene, being only ∼1 nm thick, is not visible in the cross-section images. (i) Photograph of a polymer film coated graphene membrane mounted with aluminum foil tape for gas permeance measurements.

$R_{\text{Graphene}} \approx R_{\text{PCTEM}}$, thereby increasing the likelihood of realizing a selective membrane.

3.3. Polymer film support resistance tuning

Instead of modifying the PCTEM, the support resistance was increased by adding a gas flow resistance in series with each PCTEM pore resistance (figure 5(a)). This was accomplished by depositing a thin, permeable polymer film over the graphene (figure 2(a)). Gas permeates the film (figure 1(a)) and resistance to gas flow through this layer is controlled by its thickness. Polydimethylsiloxane (PDMS) was selected for this polymer because it has relatively high permeability [37] while only requiring simple fabrication steps to deposit a thin film. Gas flow rate measurements show that adding a PDMS layer to the PCTEM raises the gas resistance (lowers the permeance) of the support by of factor of $\sim 10^5$ (figure 5(b)).

Unlike in the well-defined PCTEM pores, in the PDMS layer, gas flow is able to spread laterally, as illustrated in figures 5(c)–(e). It is therefore essential that the polymer layer be thin to maintain the flow path isolation achieved by the PCTEM. That is, if the PDMS thickness is sufficiently smaller than the average tear spacing in graphene, gas leakage flow through tears will be restricted to that portion of the flow entering isolated areas on the film surface (figure 5(e)). Gas flow through other areas will pass through the PDMS layer, (porous) graphene, and the support pore, since the resistance path from areas with graphene, laterally through the PDMS layer, to a tear will be much higher than that through the graphene and into the support pore. Conversely, if the PDMS thickness is larger than the spacing between tears, gas flow entering through any area on the PDMS will have a low resistance pathway through a tear (figure 5(d)); in such a scenario, the tear isolation properties of the PCTEM will be lost, increasing the contribution of gas leakage through the membrane.

The pore density in the 200 nm PCTEMs is 3×10^8 pores cm^{-2}, which corresponds to an average spacing between PCTEM pores of 580 nm. The single layer graphene coverage of approximately 70% (figure 3(c)) implies an average spacing between tears of 1050 nm, if the tears are evenly distributed. This is less than the PDMS film thickness over graphene of approximately 1500 nm, measured in SEM cross-sections of the membrane (figures 5(f)–(h)). In order to produce thinner PDMS films we explored spin coating PDMS diluted in heptane on the membrane. While films down to ∼100 nm were produced, these layers were found to have pinhole defects. Although these defects covered <1% of the membrane area, they completely compromised the resistance matching ability of the film. For this reason, 1500 nm thick films were used.

Gas flow measurements are consistent with the above mechanism, which suggests that this film is too thick to be effective. Specifically, without a PDMS film, transferring

graphene onto a PCTEM reduced leakage by ~70% (figure 3(c)). However, a single layer graphene membrane with PDMS coating, shown mounted for measurement in figure 5(i), has only approximately 20% lower leakage than a PCTEM coated with PDMS (without graphene). In other words, leakage through tears is the dominant transport pathway of least resistance and the graphene is not governing the gas transport; even if perfectly selective pores could be introduced into the graphene, their contribution to transport compared to leakage would be small, having little effect on overall membrane selectivity. Ideally, PDMS-coated graphene on PCTEM would have a significantly lower flow rate before pore creation than that of the PDMS-coated PCTEM without graphene, so that the graphene layer governs transport. These results show that the 1500 nm thick PDMS layer is too thick compared to the tear spacing in single layer graphene.

Two layer graphene, with ~88% coverage (figure 3(c)), has an average tear spacing of ~1700 nm, similar to the PDMS thickness, and will therefore also suffer from leakage due to flow spreading in the polymer layer. On the other hand, three layer graphene has a coverage of ~99% (figure 3(c)), corresponding to an average tear spacing of ~5800 nm, much larger than the PDMS film thickness. Three layers of graphene reduced leakage by ~90% compared to a PDMS-coated PCTEM without graphene (figure 5(b)). In other words, graphene is significantly impeding leakage flow. Furthermore, there is sufficient permeance difference between membranes with and without graphene that the potential exists to increase overall membrane selectivity by introducing selective pores. Thus, three layer membranes with PDMS film coating were selected for further study. The lower leakage reduction for three layer membranes with PDMS (~90%) compared to membranes without PDMS (~99%) may be a result of flow spreading in the PDMS; PCTEM pores beneath tears have an effectively higher open area when covered in PDMS due to flow spreading in the high resistance polymer film, increasing the relative leakage flow through these areas.

SEM cross-section images of PDMS on graphene reveal an important feature of the membrane structure. PCTEM pores beneath tears in the graphene appear to fill with PDMS (figure 5(c)), locally increasing the gas flow resistance where there would otherwise be high leakage. The images in figures 5(f)–(h) show PDMS over a low-quality graphene transfer, which has millimeter-scale gaps in the graphene coverage. The lower half of the cross-section image in figure 5(h) shows an area with graphene whereas the top half shows an area without graphene. Open PCTEM pores are visible in areas with graphene (figure 5(f)). Pores are not visible in areas without graphene coverage (figure 5(g)), suggesting that they have been filled with the polymer.

3.4. Membrane performance

Membranes consisting of three-layer graphene over 200 nm pore PCTEMs were bombarded at various ion densities and then spin-coated with PDMS (figure 2(a)). Flow rate measurements show a significant increase in membrane permeance between 10^{14} and 10^{15} ion cm^{-2} bombardment (figure 6(a)), consistent with measurements without PDMS (figures 4(b), (c)). The flow rate ratio is smaller for PDMS-coated three-layer membranes (~1.8, figure 6(b)) compared to non-coated membranes (~4.9, figure 3(g)). The reason for this is that the PDMS film has a low gas selectivity of ~1.8 and has a high resistance, causing a greater portion of the leakage flow to be through micron-scale tears than through nanometer-scale defects in graphene due to flow spreading in the PDMS. However, gas flow measurements (figure 6(b)) show that by tuning the ion bombardment density, selectivity can be increased from ~1.8, that of the PDMS, to ~5.7, near the Knudsen selectivity (~6.0). This demonstrates selective gas transport through ion perforated graphene membranes at centimeter-scale.

Graphical explanation for the observed trends is provided in figures 6(c)–(e). At low bombardment densities (~10^{14} ion cm^{-2}, figure 6(c)), the dominant flow path is through PDMS filled tears in the membrane. As a result, the permeance is low (figure 6(a), blue region) and the selectivity is that of the PDMS (figure 6(b), blue region). At moderate bombardment densities (~10^{15} ion cm^{-2}, figure 6(d)), the graphene permeance becomes significant compared to that through tears. Membrane flow rate increases (figure 6(a), green region) as does selectivity (figure 6(b), green region). At high bombardment densities (>2×10^{15} ion cm^{-2}, figure 6(e)), the graphene is destroyed. The support pores fill with PDMS during spin coating resulting in a drop in flow rates (figure 6(a), red region) and the selectivity returning to the value for PDMS (figure 6(b), red region).

The maximum flow rate through the PDMS-coated graphene membrane is higher than the value obtained for a PDMS-coated PCTEM without graphene, that is, the normalized flow rate is greater than 1 (figure 6(a)). This is consistent with the observed PDMS filling of all PCTEM support pores beneath tears. In membranes without graphene, all support pores are filled by PDMS. On the other hand, in a membrane with graphene, PDMS will only fill PCTEM pores that are sufficiently exposed due to large tears in the overlying graphene. Ion bombardment can create pores in the graphene that are gas permeable but that do not permit PDMS filling. If the graphene permeance is high enough, it is possible for the gas flow rate through these PCTEM pores to be higher than in a membrane without graphene, because the resistance to gas flow through the support is lower without PDMS filling.

An important feature of the results in figures 6(a), (b) is that, even at the optimal bombardment density (~1.1×10^{15} ions cm^{-2}), the selectivity does not exceed the Knudsen selectivity. This suggests that at bombardment density levels where the graphene is sufficiently permeable to influence overall membrane flow rates, the pores in graphene are larger than the diameter of gas molecules. This is consistent with the damage observed in three-layer graphene without PDMS at this bombardment density (~10^{15} ion cm^{-2}, figures 4(c), (d)). The results suggest that the increase in selectivity is then due to the high permeance through created nanometer-scale pores operating in a Knudsen effusion regime rather than a molecular sieving regime (figure 1(a))

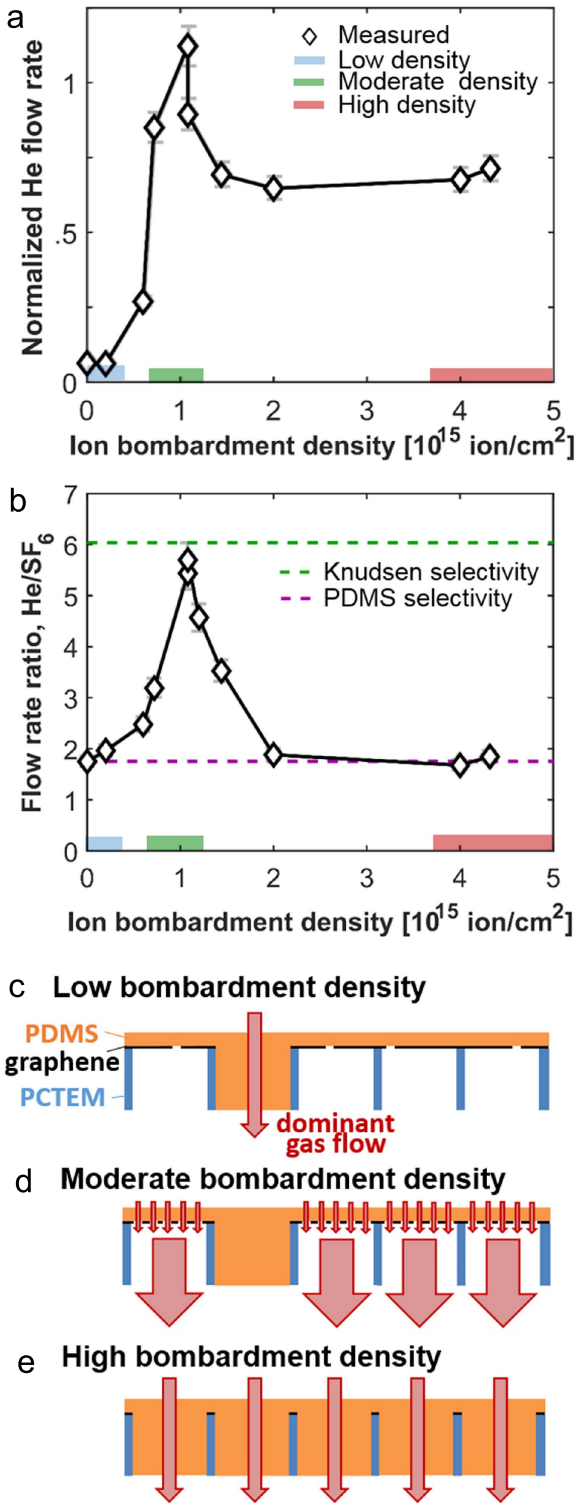

Figure 6. Selective transport through three-layer graphene membrane with a polymer film layer. (a) Helium flow rate as ion bombardment density is increased. Flow rate is normalized by that through a PCTEM with a PDMS coating and without graphene (as opposed to figures 3(c), 4(b), (c) and 5(b) where normalization is to a PCTEM without PDMS or graphene). The plotted ion bombardment density is the maximum value in any area of the membrane. Each data point is for a different membrane. (b) Corresponding He/SF_6 flow rate ratio. (c)–(e) Illustration of membrane structure for different bombardment densities. The bombardment densities corresponding to (c)–(e) are shaded in (a), (b).

and is therefore a result of differences in molecule mass rather than molecule size.

4. Discussion

Due to tear alignment between graphene layers over PCTEM pores, in a three-layer membrane, not all PCTEM pores have three layers of graphene coverage. Some have two layers, one layer, or no layers. In a membrane with approximately 70% graphene coverage per layer, 19% of the PCTEM pores have one layer of coverage, 44% have two layer coverage, and 34% have three layer coverage (approximately) [27]. Ion bombardment is likely affecting these areas differently. At a specific bombardment density, areas of single layer graphene will be perforated more than areas with three layer graphene. It is possible that areas of one-layer graphene are destroyed at bombardment densities below that at which areas of two-layer graphene develop significant permeance, and similarly for two layers compared to three layers. This is a possible explanation for the observation that, as compared to the corresponding non-bombarded membrane, at bombardment densities of order 10^{15} ion cm^{-2}, without a PDMS film coating selectivity is lower (figure 4(d)), whereas with a film coating selectivity is higher (figure 6(b)). If areas of one-layer and some areas of two-layer graphene are destroyed, leakage through these areas will dominate over that through pores in three-layer areas of graphene without a polymer film coating. However, this leakage is reduced with the high resistance polymer film coating. As a result, the permeance through the remaining two-layer areas and three-layer areas has a significant effect on the permeance, resulting in increased selectivity.

PDMS-coated PCTEMs have a helium permeance with respect to PCTEM pore area of 8.6×10^{-8} mol m^{-2} s^{-1} Pa^{-1}, which is 1.3×10^{-5} times smaller than the value of 6.5×10^{-3} mol m^{-2} s^{-1} Pa^{-1} for the uncoated PCTEM. Our results show that Knudsen selectivity, but not molecular sieving, can be achieved through porous graphene with permeance near both that of the PDMS coated PCTEM (figure 6) and non-coated PCTEM (figure 4). Based on reported single pore measurements [22], simulations [2–4, 24], and created pore densities [9, 23], we expect the achievable permeance of porous graphene exhibiting molecular sieving to be in the range of 2×10^{-6} to 2×10^{-4} mol m^{-2} s^{-1} Pa^{-1} (figure 1(b)), lower than that of the uncoated PCTEM. The failure to exceed the Knudsen selectivity in membranes without a PDMS coating is therefore not surprising. However, the results show that ion bombardment did not enable molecular sieving with permeance $\gtrsim 10^{-7}$ mol m^{-2} s^{-1} Pa^{-1}. The simultaneous occurrence of membrane areas with different numbers of graphene layers, possibility of ion bombardment making the graphene amorphous and only producing large pores, as well as the potential for PDMS to interact with pores in graphene, may have resulted in the observed behavior.

Raising membrane selectivity beyond the Knudsen selectivity will require methods to produce high graphene

permeance from smaller nanopores, or improvement of the membrane design to tolerate lower porous graphene permeance. Creating a high density of smaller pores without damaging the graphene will likely be simpler in single-layer graphene than three layer graphene. However, this will require an alternative process to match the support pore resistance to the graphene resistance. Methods that enlarge nucleated pores by etching may also result in permeable nanopores with more uniform size and with smaller damaged graphene areas [9, 23].

5. Conclusions

High density ion bombardment is able to perforate graphene, increasing its permeance. However, due to defects in large areas of graphene, significant damage must be sustained before measurably changing membrane permeance. It is possible to reduce the contribution of this leakage flow by fabricating a support structure with comparable gas flow resistance to the pores created in graphene. In this work, a thin polymer film was deposited on the graphene in an effort to achieve this matching. Unfortunately, limitations on the thickness and permeance of the layer prevented leakage mitigation in single layer graphene membranes. The layer did provide adequate leakage mitigation for three-layer graphene, where the average spacing between permeable defects is larger. Using this design, near Knudsen selectivity was measured through centimeter-scale graphene membranes. The fact that the selectivity did not exceed the Knudsen effusion limit suggests that the selective pores created in graphene are larger than the kinetic diameter of the gas molecules, such that separation is resulting from differences in molecule mass rather than molecule size. Furthermore, the relatively low permeance of the polymer film and difficulty in creating a high density of small pores in three-layer graphene result in low permeance. Single-layer graphene with effective leakage mitigation may provide an easier path to simultaneously achieve the high permeance and high selectivity, molecular-sieving based, gas separation promised by graphene membranes.

Acknowledgments

This research was funded in part by an MIT Energy Initiative seed grant and in part by the US Department of Energy Office of Basic Energy Sciences award number DE-SC0008059. MSHB acknowledges support from the Natural Sciences and Engineering Research Council of Canada (NSERC) post-graduate scholarships program. The authors acknowledge Mathias Kolle for discussions on PDMS coating, and William Koros for suggestions on sealing of membranes for gas flow measurements. This work made use of the MRSEC Shared Experimental Facilities at MIT, supported by the National Science Foundation under award number DMR-1419807.

Competing financial interests

RK discloses financial interest in a company aimed at commercializing graphene membranes.

References

[1] Bunch J S, Verbridge S S, Alden J S, Van Der Zande A M, Parpia J M, Craighead H G and McEuen P L 2008 Impermeable atomic membranes from graphene sheets *Nano Lett.* **8** 2458–62
[2] Hauser A W and Schwerdtfeger P 2012 Methane-selective nanoporous graphene membranes for gas purification *Phys. Chem. Chem. Phys.* **14** 13292
[3] Liu H, Dai S and Jiang D 2013 Permeance of H_2 through porous graphene from molecular dynamics *Solid State Commun.* **175–176** 101–5
[4] Schrier J 2010 Helium separation using porous graphene membranes *J. Phys. Chem. Lett.* **1** 2284–7
[5] Baker R W 2002 Future directions of membrane gas separation technology *Ind. Eng. Chem. Res.* **41** 1393–411
[6] Baker R W and Low B T 2014 Gas separation membrane materials: a perspective *Macromolecules* **47** 6999–7013
[7] Baker R W 2004 *Membrane Technology and Applications* (Chichester: Wiley)
[8] Cohen-Tanugi D and Grossman J C 2012 Water desalination across nanoporous graphene *Nano Lett.* **12** 3602–8
[9] Surwade S P, Smirnov S N, Vlassiouk I V, Unocic R R, Veith G M, Dai S and Mahurin S M 2015 Water desalination using nanoporous single-layer graphene *Nat. Nanotechnol.* **10** 459–64
[10] Wijmans J G and Baker R W 1995 The solution-diffusion model: a review *J. Membr. Sci.* **107** 1–21
[11] Robeson L M 2008 The upper bound revisited *J. Membr. Sci.* **320** 390–400
[12] Alexander Stern S 1994 Polymers for gas separations: the next decade *J. Membr. Sci.* **94** 1–65
[13] Bernardo P, Drioli E and Golemme G 2009 Membrane gas separation: a review/state of the art *Ind. Eng. Chem. Res.* **48** 4638–63
[14] Sanders D F, Smith Z P, Guo R, Robeson L M, McGrath J E, Paul D R and Freeman B D 2013 Energy-efficient polymeric gas separation membranes for a sustainable future: a review *Polymer* **54** 4729–61
[15] Yampolskii Y 2012 Polymeric gas separation membranes *Macromolecules* **45** 3298–311
[16] Strathmann H 1981 Membrane separation processes *J. Membr. Sci.* **9** 121–89
[17] Liu G, Jin W and Xu N 2016 Two-dimensional-material membranes: a new family of high-performance separation membranes *Angew. Chem., Int. Ed.* **55** 13384–97
[18] Shen J, Liu G, Huang K, Chu Z, Jin W and Xu N 2016 Subnanometer two-dimensional graphene oxide channels for ultrafast gas sieving *ACS Nano* **10** 3398–409
[19] Nair R R, Wu H A, Jayaram P N, Grigorieva I V and Geim A K 2012 Unimpeded permeation of water through helium-leak–tight graphene-based membranes *Science* **335** 442–4
[20] Celebi K, Buchheim J, Wyss R M, Droudian A, Gasser P, Shorubalko I, Kye J-I, Lee C and Park H G 2014 Ultimate

permeation across atomically thin porous graphene *Science* **344** 289–92
[21] Schofield R W, Fane A G and Fell C J D 1990 Gas and vapour transport through microporous membranes: I. Knudsen–Poiseuille transition *J. Membr. Sci.* **53** 159–71
[22] Koenig S P, Wang L, Pellegrino J and Bunch J S 2012 Selective molecular sieving through porous graphene *Nat. Nanotechnol.* **7** 728–32
[23] O'Hern S C, Boutilier M S H, Idrobo J C, Song Y, Kong J, Laoui T, Atieh M and Karnik R 2014 Selective ionic transport through tunable subnanometer pores in single-layer graphene membranes *Nano Lett.* **14** 1234–41
[24] Sun C, Boutilier M S H, Au H, Poesio P, Bai B, Karnik R and Hadjiconstantinou N G 2014 Mechanisms of molecular permeation through nanoporous graphene membranesseparation *Langmuir* **30** 675–82
[25] Celebi K, Buchheim J, Wyss R M, Droudian A, Gasser P, Shorubalko I, Kye J-I, Lee C and Park H G 2014 Ultimate permeation across atomically thin porous graphene *Science* **344** 289–92
[26] Breck D W 1974 *Zeolite Molecular Sieves: Structure, Chemistry, and Use* (New York: John Wiley and Sons)
[27] Boutilier M S H, Sun C, O'Hern S C, Au H, Hadjiconstantinou N G, Karnik R, O'Hern S C, Au H, Hadjiconstantinou N G and Karnik R 2014 Implications of permeation through intrinsic defects in graphene on the design of defect-tolerant membranes for gas separation *ACS Nano* **8** 841–9
[28] O'Hern S C, Stewart C A, Boutilier M S H, Idrobo J-C, Bhaviripudi S, Das S K, Kong J, Laoui T, Atieh M and Karnik R 2012 Selective molecular transport through intrinsic defects in a single layer of CVD graphene *ACS Nano* **6** 10130–8
[29] Ambrosi A, Bonanni A, Sofer Z and Pumera M 2013 Large-scale quantification of CVD graphene surface coverage *Nanoscale* **5** 2379
[30] Schriver M, Regan W, Gannett W J, Zaniewski A M, Crommie M F and Zettl A 2013 Graphene as a long-term metal oxidation barrier: worse than nothing *ACS Nano* **7** 5763–8
[31] Bunch J S, Verbridge S S, Alden J S, van der Zande A M, Parpia J M, Craighead H G and McEuen P L 2008 Impermeable atomic membranes from graphene sheets *Nano Lett.* **8** 2458–62
[32] Li H, Song Z, Zhang X, Huang Y, Li S, Mao Y, Ploehn H J, Bao Y and Yu M 2013 Ultrathin, molecular-sieving graphene oxide membranes for selective hydrogen separation *Science* **342** 95–8
[33] Moore T T, Damle S, Williams P J and Koros W J 2004 Characterization of low permeability gas separation membranes and barrier materials; design and operation considerations *J. Membr. Sci.* **245** 227–31
[34] Lehtinen O, Kotakoski J, Krasheninnikov A V, Tolvanen A, Nordlund K and Keinonen J 2010 Effects of ion bombardment on a two-dimensional target: atomistic simulations of graphene irradiation *Phys. Rev.* B **81** 153401
[35] Lehtinen O, Kotakoski J, Krasheninnikov A V and Keinonen J 2011 Cutting and controlled modification of graphene with ion beams *Nanotechnology* **22** 175306
[36] O'Hern S C, Jang D, Bose S, Idrobo J-C, Song Y, Laoui T, Kong J and Karnik R 2015 Nanofiltration across defect-sealed nanoporous monolayer graphene *Nano Lett.* **15** 3254–60
[37] Nunes S P and Peinemann K-V 2001 Gas separation with membranes *Membrane Technology: in the Chemical Industry* ed S P Nunes and K-V Peinemann vol 0 (Weinheim, FRG: Wiley-VCH Verlag GmbH) 6